A molecularly imprinted antibiotic receptor on magnetic nanotubes for the detection and removal of environmental oxytetracycline

Wang, Jixiang; Li, Xiaolei; Zhang, Rong; Fu, Bingjie; Chen, Mingcan; Ye, Mengxue; Liu, Wanyu; Xu, Jingjing; Pan, Guoqing; Zhang, Hongbo

Published in:
Journal of Materials Chemistry. B

DOI:
10.1039/D2TB00497F

Published: 21/09/2022

Document Version
Accepted author manuscript

Document License
Publisher rights policy

A molecularly imprinted antibiotic receptor on magnetic nanotubes for the detection and removal of environmental oxytetracycline

Jixiang Wang,‡[abc] Xiaolei Li,‡[a] Rong Zhang,[d] Bingjie Fu,[a] Mingcan Chen,[a] Mengxue Ye,[a] Wanyu Liu,[a] Jingjing Xu, *[a] Guoqing Pan *[e] and Hongbo Zhang *[bc]

Abstract: The detection and elimination of antibiotic contaminants, such as oxytetracycline (OTC), a broad- spectrum tetracycline antibiotic, would be of help in efficient environmental monitoring, agriculture and food safety tests. Nevertheless, currently available methodologies, which mostly rely on the chromatographic separation of OTC, suffer from low sensitivity and complicated processes. Thus, we report here on the design and synthesis of a fluorescent sensor based on molecularly imprinted magnetic halloysite nanotubes (referred to as MHNTs@FMIPs) for the effective detection and purification of OTC in actual environmental samples. The fluorescence of the MHNTs@FMIPs was quenched obviously upon loading with OTC, covering a linear concentration range of 10–300 nM with a limit of detection (LOD) as low as 8.1 nM. The imprinting factor is 4.47, indicating an excellent specificity. Furthermore, the MHNTs@FMIPs can be applied to the quantitative detection of OTC (5 cycles of 300 nM) in aquaculture wastewater and Yangtze River water, demonstrating their immense application potential.

[a] Sino-European School of Technology of Shanghai University, Shanghai University, CN-200444, Shanghai, P. R. China. E-mail: jingjing_xu@shu.edu.cn
[b] Pharmaceutical Sciences Laboratory, Åbo Akademi University, FI-20520, Turku, Finland. E-mail: hongbo.zhang@abo.fi
[c] Turku Bioscience Centre, University of Turku and Åbo Akademi University, FI-20520, Turku, Finland
[d] Department of Interventional Radiology, Shanghai Jiao Tong University Affiliated Sixth People's Hospital, CN-200233, Shanghai, China
[e] Institute for Advanced Materials, School of Materials Science and Engineering, Jiangsu University, Zhenjiang, 212013, Jiangsu, China. E-mail: panguoqing@ujs.edu.cn
‡ These authors contributed equally to this work.

1. Introduction

Since the landmark work in the 1960s on the development of glucose sensors and lateral flow devices such as pregnancy test kits, research on biosensors has experienced incredible success, which has led to more attention on accurate and robust biosensor development for real sample examination.[1] Following the outbreak of the novel coronavirus disease (COVID-19), humans have become soberly aware of the fact that a great deal of infectious diseases originate from the environment and enter through the mouth, hence the impor- tance of environmental monitoring and food safety control.[2,3]

The threat of virus/bacterial infections to human health has attracted worldwide attention since the beginning of history, for which the treatment mainly relies on the use of antibiotics. In this regard, people began to blindly pursue ''getting better soon'' and ''making more money'', leading to the abuse of antibiotics. In turn, antimicrobial resistance in microorgan- isms has spread widely, which is a public health problem facing the world, and might cause 10 million global deaths each year by 2050.[4] Therefore, there is an unmet demand for sensitive, rapid and selective sensors for antibiotics that would allow robust environmental monitoring and ensure food quality.[5,6] However, achieving this ambition faces three main challenges, which are assay sensitivity, selectivity and long detection time.[7] One promising tactic to gain greater sensitivity is to confine the sensor to the nanoscale.[8] In addition, magnetic properties could be integrated, thereby closing the distance between the detector and the analytes, leading to a rapid response.[9,10] Moreover, if the biosensor was designed as a specific biorecog- nition element integrated signal transducer, it would be suita- ble for selective and on-site tests in real samples, for which there are many examples, the fluorescent nanoprobe being the most notable of these.[11–13]

For the design of nanostructures with distinct layers and excellent functions, the selection of building blocks is of primary importance.[14–16] Halloysite nanotubes (HNTs), a clay

aluminosilicate mineral, exhibiting several elegant properties such as strong interactions, good dispersibility, and large surface area, have gained enormous interest in recent years.[17] In contrast with other nanosized materials, like carbon nanoparticles,[18,19] metal–organic frameworks,[14,20] and quantum dots,[15,16,21,22] HNTs are available in thousands of tons at a low price, making them a promising candidate for nanoarchitecture composites. A classic example is the magnetic HNTs (MHNTs), onto which Fe_3O_4 can be adsorbed due to the abundant hydroxyl groups on the surface of the HNTs.[23] Using the MHNTs as a building block, a robust recognition element with antibody-like affinity to specifically detect analytes can nowadays be tailor-made using molecular imprinting technology,[24–26] hence the interest in creating a molecularly imprinted polymer (MIP) layer on MHNTs.

For the detection of environmental pollutants, oxytetracycline (OTC) was selected as an example in this study. OTC is a sort of broad-spectrum antibiotic belonging to the tetracycline family and has been extensively applied for the prevention and control of infections in the livestock industry, thus leading to pollution of soils and surface water.[27] The detection and separation of OTC mainly rely on chromatographic separation columns, which are limited by their high-cost, long detection time and low recovery rate.[28] Therefore, we have developed a fluorescence sensor here for cost-effective, specific, quantitative detection and extraction of OTC in real samples (Scheme 1).[29–33] Moreover, the MIP-based fluorescent sensor was designed to achieve nM level sensitivity, like MIP-based screen printed electrodes for penicillin detection *via* measuring the thermal resistance difference at the solid–liquid interface, MIP-based 3D-printed flow cells for nafcillin detection using a combined thermal and fluorescence device, *etc.*[34,35] First, HNTs were used as a building block, and were then combined with Fe_3O_4 nanoparticles through their surface hydroxyl groups, so as to speed up the detection time and facilitate the extraction. Afterwards, a fluorescent MIP layer was synthesized onto the MHNTs, using methacrylic acid (MAA) and allyl rhodamine B (ARhB, a polymerizable fluorophore) as functional monomers to exhibit hydrogen bonding and boron affinity toward OTC, respectively. The polymer was finally generated through the cross-linking of ethylene glycol dimethacrylate (EGDMA). Subsequent to the extraction of entrapped OTC, the obtained MHNTs@MIPs were applied for OTC detection in farming wastewater and Yangtze River water, *via* a fluorescence quenching mechanism.

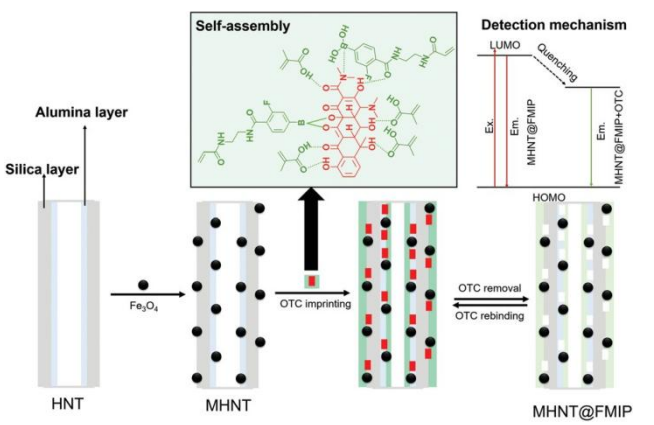

Scheme 1. Schematic illustration of the preparation of MHNTs@FMIPs and their detection mechanism.

2. Experimental section

2.1. Reagents

3-(Methacryloxyl) propyl trimethoxysilane (KH-570, 98%), ethylene glycol dimethacrylate (EGDMA, 98%), 2,2^0-azobis (isobutyronitrile) (AIBN, 99%), tetracycline (TC, analytical standard), amoxicillin (AMO, Z98%), levofloxacin (LEV, 95%), doxorubicin hydrochloride (DOX, 98%), rhodamine B (RhB, Z99.0%), oxytetracycline (OTC, Z98%), and chlorotetracycline hydrochloride (CTC, analytical standard) were all purchased from Aladdin Reagent Co., Ltd. (Shanghai, China). *N*,*N*-Dimethylformamide (DMF, Z99.5%), methacrylic acid (MAA, Z99.0%), tetrahydrofuran (THF, Z99.8%), toluene (Z99.5%), ethylene glycol (Z99.0%), 4-carboxy-3-fluorophenylboronic acid (98%), thionyl chloride (Z99.0%), N-carboxybenzyloxy- 1,2-diaminoethane hydrochloride (98.0%), Na_2CO_3 (Z99.8%), trimethylammonium (99%), acrylic chloride (97%), halloysite nanotubes (HNTs, 99%), Fe $(NO_3)_3$·$9H_2O$ (Z98.5%) and acetone (Z99.0%) were obtained from Sinopharm Chemical Reagent Co., Ltd. (Shanghai, China). Double-distilled ultrapure water was purified with a Purelab ultra (Organo, Tokyo, Japan).

2.2. Preparation of magnetic halloysite nanotubes (MHNTs)

To prepare the building block, Fe3O4 was loaded onto the surface of halloysite nanotubes (HNTs), to obtain mag- netic halloysite nanotubes (MHNTs). Specifically, 1 g of HNTs was ultrasonically dispersed in 20 mL of ethanol and stirred vigorously. 0.6 g Fe (NO3)3·9H2O was then added into the reaction mixture, which was stirred at room temperature for 10 h. Afterward, the reaction mixture was placed in a vacuum drying oven at 90 1C for 2 h. Following this, the crude product was completely immersed in ethylene glycol, and placed in a tube furnace under a N_2 atmosphere at 400 1C (heating rate: 5.0 1C min ^{1}) for 2.0 h. At the end, the final product MHNTs were taken out for further use.

2.3. Preparation of vinyl modified MHNTs

To make vinyl-modified MHNTs, KH-570 was used, so as to facilitate the subsequent polymerization reaction. Briefly, 2 g of MHNTs were ultrasonically dispersed in 100 mL of dry toluene. Then, 2 mL of KH-570 was slowly added into the MHNT dispersion, which was stirred at 90 1C for 24 h. After centrifuga- tion and washing with toluene several times, the final product was obtained by drying at 60 1C for 10 h.

2.4. Preparation of MHNTs@FMIPs

For the purpose of imprinting OTC on the vinyl-modified MHNTs, 50.0 mg of ARhB (Fig. S1, synthesis details in ESI†), 25.8 mg of MAA, 56.0 mg of AFPBA (Fig. S2, synthesis details in

ESI†) and 49.7 mg of OTC were dispersed in 20 mL of acetonitrile, and pre-assembled for 2.0 h in a dark environment. At the same time, 100 mg of KH-570 modified MHNTs was ultrasonically dispersed in 30 mL of acetonitrile, and then poured into the pre-assembled system. Afterwards, 256.2 mg of EGDMA was added dropwise with stirring. After AIBN addition, the reaction mixture was bubbled with sufficient N_2 to completely remove the residual oxygen. Then, the whole system was reacted in a water bath at 60 1C for 24 h with stirring. After the reaction, the final product MHNTs@FMIPs were obtained by external magnet separation, ethanol and acetonitrile wash- ing, and 60 1C dying for 10 h. During the washing process, the OTC was removed by solvent elution through a Soxhlet extractor. The MHNTs@FNIPs were prepared by following the same protocol in the absence of OTC.

2.5. Characterization of the MHNTs@FMIPs

The characterization of the HNTs, MHNTs and MHNTs@FMIPs was sequentially carried out by Fourier-transform infrared spectroscopy (FT-IR, equipped with a KBr pellet in a Nicolet NEXUS-470 apparatus, PerkinElmer Frontiert, USA) for composition analysis, transmission electron microscopy (TEM, JEOL, JEM-2100, Japan) for size and morphology obser- vation, and vibrating sample magnetometer (VSM, Princeton Optronics, Inc., USA) for verifying magnetism. For fluorescence analysis, a Cary Eclipse fluorescence spectrophotometer (Varian, USA) was employed.

2.6. Application of the MHNTs@FMIPs for OTC detection

Specificity test. The fluorescence measurements were carried out at room temperature with excitation at 540 nm. First, 30 mg L^{-1} MHNTs@FMIPs or MHNTs@FNIPs were incubated with OTC ranging from 0 to 1.5 mM for 15 min. Afterward, the fluorescence spectra were recorded in the range of 550–800 nm, and the fluorescence quenching rate ($F_0/F - 1$) was calculated using the emission values at 575 nm.

Selectivity test. Three structural analogues, namely doxorubicin (DOX), levofloxacin (LEV) and amoxicillin (AMO), as well as two kinds of tetracycline, namely tetracycline (TC) and chlorotetracycline (CTC), were used for comparison with the OTC detection performance. 30 mg L^{-1} MHNTs@FMIPs or MHNTs@FMIPs were incubated with 300 nM OTC, or DOX, or LEV, or AMO, respectively. Then, the fluorescence quenching rate of each sample was recorded.

Real sample detection. Farming wastewater (taken from a breeding base in Zhenjiang) and Yangtze River water (taken from the Yangtze River Basin in Jiangsu) were selected as real samples for the OTC recovery experiments. Then, a standard recovery method was adopted, using a calibration plot. For spiked sample preparation, an OTC standard at concentrations ranging from 20 to 600 nM was prepared either in farming wastewater or Yangtze River water, for the determination of the recovery. The samples were treated by a syringe filter (diameter: 0.22 mm) to remove insoluble impurities or proteins before fluorescence measurements.

3. Results

3.1. Characterization of the MHNTs@FMIPs

The preparation process of the MHNTs@FMIPs is illustrated in Scheme 1. First, the HNTs with Fe_3O_4 modification were used as building blocks for MHNTs. Then, MHNTs@FMIPs were fabricated by using ARhB (Fig. S3, ESI†) as a fluorophore, AFPBA (Fig. S4, ESI†) and MAA as functional monomers, and EGDMA as the cross-linking agent. In the imprinted cavity, MAA established hydrogen bonds with the carbonyl and hydro- xyl groups of OTC. At the same time, AFPBA bound OTC by forming intermolecular B–N coordination and boronate ester bonds. By using the solvent elution method, the intermolecular hydrogen bonds, B–N coordination and boron affinity were broken, thus releasing OTC from the imprinted cavity, leaving the specific recognition site. In this way, the final product MHNTs@FMIPs might not only specifically detect OTC, but also extract OTC from the real sample *via* a magnetic response. Hopefully, the MHNTs@MIPs can be reused several times with excellent stability, due to their reversible molecular recognition reaction and magnetism, which might bring simplicity of the identification and effectiveness of the separation.

To verify the successful generation of MHNTs, vinyl-modified MHNTs and MHNTs@FMIPs, FT-IR analysis was carried out (Fig. 1(A)). According to the absorption peak at 534 cm^{-1} in curves a, b and c, the magnetic Fe_3O_4 nanoparticles were successfully loaded onto the MHNTs, vinyl-modified MHNTs and MHNTs@FMIPs. In addition, the characteristic adsorption peak at 1637 cm^{-1} in curve b was the stretching vibration peak of a C=O double bond, indicating the presence of vinyl groups. Moreover, the characteristic absorption peak of fluoride F–Ph in the MHNTs@FMIPs appeared at 1297 cm^{-1} curve c, demonstrating the incorporation of AFPBA. Meanwhile, the flexural vibration peak of the CH bond at 1450 cm^{-1}, the skeleton vibration peak of the CC in the benzene ring at 1560 cm^{-1}, and the stretching vibration peak of the ester group

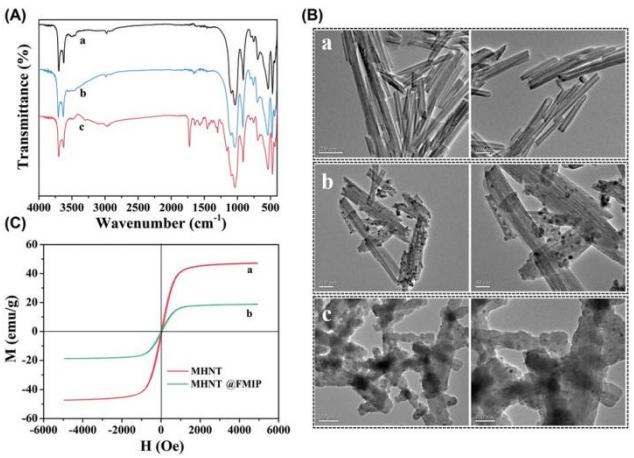

Fig. 1 (A) FT-IR spectra of the MHNTs (a), vinyl-modified MHNTs (b) and MHNTs@FMIPs (c). (B) TEM images of the HNTs (a), MHNTs (b) and MHNTs@FMIPs (c). (C) Magnetization curve of the MHNTs (a) and MHNTs@FMIPs (b).

CQO at 1724 cm^{-1} were observed in curve c, indicating that the MHNTs@FMIPs were perfectly prepared.

The morphology and dimensions of the HNTs, MHNTs and MHNTs@FMIPs were investigated by TEM. In Fig. 1(B), the HNTs showed a rod-like structure with a smooth surface. Specifically, the average tube diameter of the HNTs was about 65 nm. Moreover, Fe_3O_4 nanoparticles (diameter: B12 nm) were successfully loaded onto the surface and inside of the HNTs, while maintaining the intact structure of the HNTs. In (c), a layer of imprinted polymer (thickness: B22 nm) was wrapped on the MHNTs, leading to a tubular diameter increase. Meanwhile, the Fe_3O_4 nanoparticles were all buried inside the imprinted layer. Though some agglomeration appeared during polymerization, the surface morphology of the MHNTs@FMIPs was basically unchanged, indicating an unaffected detection specificity.

Fig. 1(C) shows the hysteresis loops of the MHNTs and MHNTs@FMIPs. Since no obvious hysteresis was observed in curve a and b, both the MHNTs and MHNTs@FMIPs were superparamagnetic. In curve a, the Ms value of the MHNTs was found to be 47.33 emu g^{-1}, indicating that Fe_3O_4 nanoparticles were successfully loaded onto the HNT interface. In addition, the Ms value of the MHNTs@FMIPs in curve b became 18.83 emu g^{-1}, due to the covering of the FMIP layer, which slightly affected the magnetism. Nevertheless, the synthesized MHNTs@FMIPs still possessed good magnetic separation performance.

3.2. Optimization of the fluorescence detection conditions

Prior to the application of the MHNTs@FMIPs, the fluores- cence detection system was optimized in detail, so as to have the ideal sensitivity conditions, while maintaining a high-quality signal intensity. First of all, the optimal concentration of the MHNTs@FMIPs was investigated in the range of 5.0– 50 mg L^{-1}, by a fluorescence quenching rate test toward 300 nM OTC. As shown in Fig. 2(A), the fluorescence quenching rate ($F_0/F - 1$, where F_0 is the original fluorescence intensity of the MHNTs@FMIPs, and F represents the fluorescence intensity of the MHNTs@FMIPs + OTC) showed a parabolic trend as the MHNT@FMIP concentration increased. The maximum fluorescence quenching rate was observed using MHNTs@FMIPs at 25 mg L^{-1}. However, the relative fluorescence intensity (F/F_0) was proportional with respect to the concentration of MHNTs@FMIPs. Therefore, in order to take into account both the fluorescence quenching rate and the relative fluorescence intensity, the intersection of the two curves was selected as the optimal MHNT@FMIP concentration, which was 30 mg L^{-1}.

Since the pH value might have an impact on the fluorescence performance of the fluorophore ARhB, the fluorescence intensities of the MHNTs@FMIPs and MHNTs@FNIPs were measured in buffers at pH values ranging from 3 to 13. As shown in Fig. 2(B), in an acidic environment, the fluorescence intensities of the MHNTs@FMIPs and MHNTs@FNIPs were significantly weaker. This was because the ARhB was quenched by H^+ caused by the carboxyl protonation effect. When the pH value was in the range of 6.0–10, the fluorescence intensity was relatively high and stable in both cases, indicating the

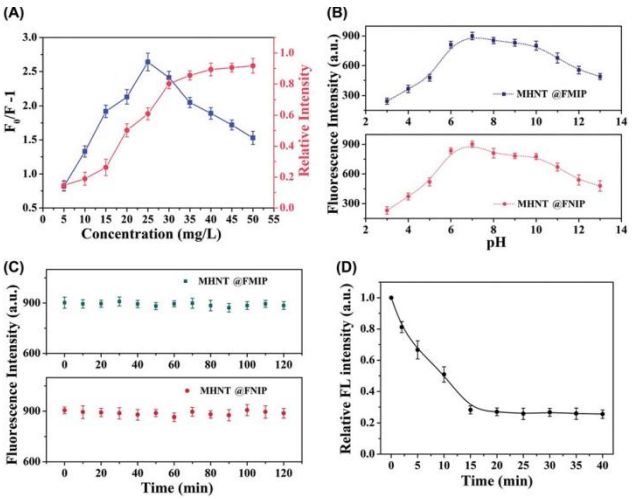

Fig. 2 Optimization studies of different experimental conditions for the fluorescence detection of OTC. (A) Effect of the MHNT@FMIP concentration on the fluorescence detection performance. Square point: the fluorescence quenching rate *versus* MHNT@FMIP concentration. Bold dots: relative fluorescence intensity *versus* MHNT@FMIP concentration. (B) Effect of pH conditions on the fluorescence intensity of the MHNTs@FMIPs and MHNTs@FNIPs. (C) Fluorescence intensity record of the MHNTs@FMIPs and MHNTs@FNIPs during 120 min. (D) Fluorescence response time of the MHNTs@FMIPs to OTC.

appropriate pH range. However, when the pH value was higher than 10, the fluorescence intensity decreased rapidly in both cases. Probably, the ARhB was degraded to some degree under the alkaline conditions. It should be noted that the fluorescence intensities of the MHNTs@FMIPs and MHNTs@FNIPs reached the maximum at pH 7. Moreover, the synthesized functional monomer AFPBA may exhibit a strong boron affinity in a neutral environment, which enhanced the importance of a neutral pH.

Fig. 2(C) shows the optical stability of the MHNTs@FMIPs and MHNTs@FNIPs. The results demonstrated that the fluorescence intensity of the MHNTs@FMIPs and MHNTs@FNIPs remained stable during 120 min (measured 13 times at an interval of 10 min). Then, the fluorescence response time of the MHNTs@FMIPs toward OTC was studied. As shown in Fig. 2(D), 30 mg L^{-1} of MHNTs@FMIPs was mixed with 300 nM of OTC, and immediately the fluorescence intensity was measured at different time intervals during 40 min. The relative fluorescence intensity (F/F_0) gradually decreased within 15 min, and remained basically stable afterwards. As a short summary, the obtained results show that the optimal MHNT@FMIP concentration was 30 mg L^{-1}, the ideal pH should be set at 7, and measurements could be quickly carried out after 15 min of incubation.

3.3. Detection performance analysis

Under the optimized conditions, the fluorescence detection performance of the MHNTs@FMIPs was investigated at room temperature. The fluorescence spectra of 30 mg L^{-1} MHNTs@- FMIPs and MHNTs@FNIPs upon OTC recognition were recorded in Fig. 3(A and B), where the fluorescence quenching

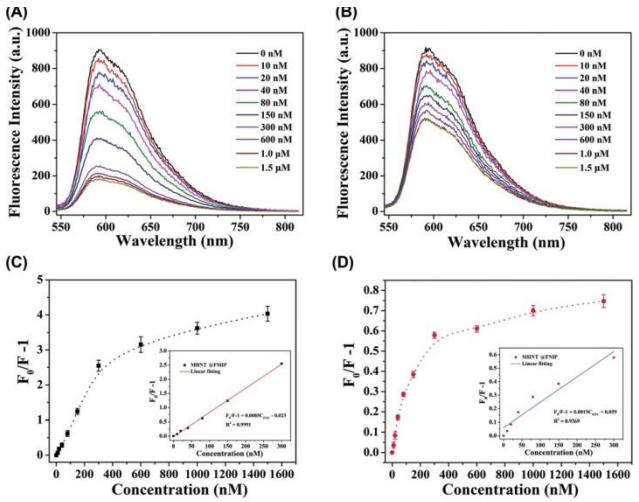

Fig. 3 (A) The fluorescence response curves of the MHNTs@FMIPs (a) and MHNTs@FNIPs (b) to OTC ranging from 0 to 1.5 mM. (B) Fluorescence quenching rate of the MHNTs@FMIPs (a) and MHNTs@FNIPs (b) *versus* the OTC concentration.

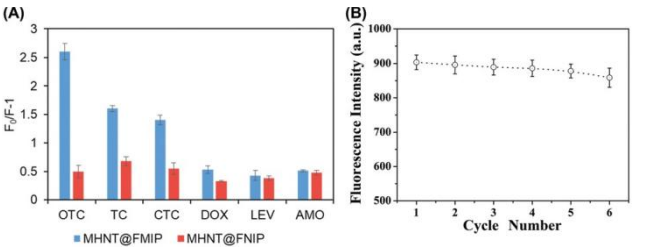

Fig. 4 (A) Study of the fluorescence quenching rate of MHNTs@FMIPs and MHNTs@FNIPs toward six analytes. (B) Durability of the MHNTs@FMIPs. Data are the mean of triplicate experiments. The error bars represent standard deviations.

phenomenon was observed in both cases. Moreover, the fluorescence quenching rate of the MHNTS@MIPS was more significant with respect to the MHNTS@NIPs, demonstrating the successful creation of specific binding sites. Specifically, the fluorescence intensity of the MHNTs@FMIPs was quenched more toward OTC within 300 nM, with respect to that superior to 300 nM. For comparison, the fluorescence quenching rate of the MHNTs@FNIPs was 5 times lower than that of the MHNTs@FMIPs. To gain insight into the fluorescence quenching mechanism, the Stern–Volmer equation: $F_0/F - 1 = k_q \times t_0 \times [C] = K_{sv} \times [C]$ was used, where kq represents the quencher rate coefficient, t_0 is the fluorescence lifetime of the fluorophore without the presence of the quencher, K_{SV} is the Stern–Volmer dynamic quenching constant, and [*C*] indicates the concentration of the quencher. As shown in Fig. 3(C and D), there was a good linear relationship between the fluorescence quenching rate of the MHNTs@FMIPs and the OTC concentration. The linear equation obtained by the MHNTs@FMIPs was $F_0/F - 1 = 0.0085[C] - 0.023$ with R^2 of 0.9991, giving a K_{SV} value of 0.0085. In the case of the MHNTs@FNIPs, the fitted linear equation was found to be $F_0/F - 1 = 0.0019[C] + 0.059$ with R^2 of 0.9057, providing a K_{sv} of 0.0019. Thus, the calculated IF ($K_{SV(MHNT@FMIP)}/K_{SV(MHNT@FNIP)}$) was found to be 4.47. Moreover, according to the equation: $D = 3s/k$ (where s is the relative standard deviation of the blank sample, and k is the slope of the calibration line), the LOD of the MHNTs@FMIPs was found to be 8.1 nM, comparable to that of the Ag-doped OTC-imprinted fluoroprobe obtained in our previous study,[9] while empowered with quantitative test potential due to the magnetic separation characteristics.

In order to study the selectivity of the MHNTs@FMIPs for OTC, three structural analogs of OTC (namely DOX, LEV and AMO), as well as two tetracyclines (namely TC and CTC), were selected for research. The fluorescence quenching rate ($F_0/F - 1$) of the MHNTs@FMIPs and MHNTs@FNIPs toward the six analytes at the concentration of 300 nmol L^{-1} is shown in Fig. 4(A). In the case of the MHNTs@FMIPs, the calculated fluorescence quenching rate was much higher for OTC, with respect to the other three structural analogs. Also, the MHNTs@FMIPs exhibited nearly two times fluorescence quenching rate for OTC, with respect to the other two tetracyclines. However, the fluorescence quenching rates of the MHNTs@FNIPs for these antibiotics were generally low. This is because OTC could quickly bind to the imprinted site, thereby enhancing the intermolecular collision with the fluorophore and accelerating electron transfer of the excited fluorophore, eventually leading to a significant fluorescence quenching.

To investigate the magnetic separation performance of the MHNTs@FMIPs, six cycles of binding and dissociation reciprocating experiments were performed. For binding purposes, 30 mg L^{-1} of MHNTs@FMIPs were used for 300 nM OTC at pH 7.0 for the fluorescence measurements. After one measurement, the OTC-bound MHNTs@FMIPs were washed with an acidic solution, separated and recovered by an external magnetic field, so as to get ready for the next cycle. As shown in Fig. 4(B), the fluorescence intensity of the MHNTs@FMIPs did not decrease significantly until the fifth cycle. However, the detection performance of the MHNTs@FMIPs was unsatisfactory in the sixth cycle, which was probably due to the partial photolysis of ARhB inside the imprinted layer. In general, the MHNTs@FMIPs showed good selectivity and regeneration performance, demonstrating their potential and reliability for real sample tests with considerable reuse cycles.

3.4. Application of the MHNTs@FMIPs for real sample detection and purification

In order to study the detection performance of the MHNTs@FMIPs in real samples, OTC standard samples (prepared in farming wastewater and Yangtze River water, respectively) at a concentration range of 20–600 nM were mixed with 30 mg L^{-1} MHNT@FMIP suspensions for incubation (pH 6.5–6.8). After incubation for 15 min, the samples were treated with a syringe filter (diameter: 0.22 mm), so as to remove insoluble impurities in the real samples. The testing results are shown in Table 1. The recovery rate of the OTC added in the real samples was relatively stable within 300 nM; however, it decreased significantly for 600 nM. This was probably because 600 nM

Table 1 Detection results of OTC in real samples by the MHNTs@FMIPs

Sample	No.	Spiked (nM)	Detected (nM)	Recovery (%)
Farming wastewater	1	20	23.6 ± 3.7	118.0 ± 18.5
	2	40	44.9 ± 6.6	112.3 ± 16.5
	3	80	86.5 ± 8.9	108.1 ± 11.1
	4	150	158.9 ± 11.2	105.9 ± 7.5
	5	300	311.8 ± 14.7	103.9 ± 4.9
	6	600	535.6 ± 41.6	89.3 ± 6.9
Yangtze river water	1	20	23.1 ± 3.5	115.5 ± 17.5
	2	40	43.7 ± 5.8	109.3 ± 14.5
	3	80	87.2 ± 9.1	109.0 ± 11.4
	4	150	159.2 ± 10.8	106.1 ± 7.2
	5	300	314.8 ± 15.4	104.9 ± 5.1
	6	600	542.6 ± 42.9	90.4 ± 7.2

was out of the linear detection range. On the other hand, the obtained recovery rates were much higher than 100% for OTC at the concentration range of 20–80 nM, due to the interferences in the real samples. Moreover, the MHNTs@FMIPs could extract 100% of 300 nM OTC from the real samples for 5 cycles. Altogether, the experimental results show the great prospects of MHNTs@FMIPs for the quantitative detection of OTC in actual environmental water.

4. Conclusion

In summary, a molecularly imprinted antibiotic receptor on magnetic halloysite nanotubes was successfully fabricated as a fluorescent sensor (MHNTs@FMIPs) and applied for quantitative detection and purification of OTC in real samples. The synthesized MHNTs@FMIPs could detect OTC at very low concentrations in real samples (LOD = 8.1 nM) with excellent stability (120 min) and repeatability (5 cycles). Moreover, the MHNTs@FMIPs presented good selectivity and 100% purification ability. Thus, we have shown the great potential of this kind of fluorescent sensor in the detection of similar antibiotics in actual environmental samples.

Author contributions

Conceptualization, writing—original draft, investigation, validation, methodology: Jixiang Wang and Xiaolei Li; assistant for methodology: Bingjie Fu, Mingcan Chen and Mengxue Ye; assistant for supervision: Rong Zhang and Wanyu Liu; conceptualization, investigation, writing—review and editing, supervision, funding acquisition: Jingjing Xu, Guoqing Pan and Hongbo Zhang. All authors have read and agreed to the published version of the manuscript.

Conflicts ofinterest

There are no conflicts to declare.

Acknowledgements

The authors acknowledge the financial support from the National Natural Science Foundation of China (21875092, 22001162), the Sigrid Juselius Foundation (28001830k1), the Academy of Finland grant (328933), and the Shanghai Sailing Program (20YF1414200). For this article, we appreciate Dr Wang Jixiang's input during his academic visit and the long-lasting friendship between China and Finland.

References

1 J. Kim, A. S. Campbell, B. E.-F. de Á vila and J. Wang, Wearable biosensors for healthcare monitoring, *Nat. Biotechnol.*, 2019, 37(4), 389–406.
2 N. Bhalla, Y. Pan, Z. Yang and A. F. Payam, Opportunities and challenges for biosensors and nanoscale analytical tools for pandemics: COVID-19, *ACS Nano*, 2020, 14(7), 7783–7807.
3 B. Tse Sum Bui, T. Auroy and K. Haupt, Fighting Antibiotic-Resistant Bacteria: Promising Strategies Orchestrated by Molecularly Imprinted Polymers, *Angew. Chem.*, 2022, 61(8), e202106493.
4 A. Gupta, S. Mumtaz, C.-H. Li, I. Hussain and V. M. Rotello, Combatting antibiotic-resistant bacteria using nanomaterials, *Chem. Soc. Rev.*, 2019, 48, 415–427.
5 O. Jamieson, F. Mecozzi, R. D. Crapnell, W. Battell, A. Hudson and K. Novakovic, *et al.*, Approaches to the rational design of molecularly imprinted polymers developed for the selective extraction or detection of antibiotics in environmental and food samples, *Phys. Status Solidi A*, 2021, 218(13), 2100021.
6 L. Zou, R. Ding, X. Li, H. Miao, J. Xu and G. Pan, Typical fluorescent sensors exploiting molecularly imprinted hydrogels for environmentally and medicinally important analytes detection, *Gels*, 2021, 7(2), 67.
7 Y. Wu, R. D. Tilley and J. J. Gooding, Challenges and solutions in developing ultrasensitive biosensors, *J. Am. Chem. Soc.*, 2018, 141(3), 1162–1170.
8 L. Jia, R. Chen, J. Xu, L. Zhang, X. Chen, N. Bi and T. Zhao, A stick-like intelligent multicolor nano-sensor for the detec- tion of tetracycline: The integration of nano-clay and carbon dots, *J. Hazard. Mater.*, 2021, 413, 125296.
9 Y. Zhang, L. Zhang, L. Yang, C. I. Vong, K. F. Chan and W. K. Wu, *et al.*, Real-time tracking of fluorescent magnetic spore–based microrobots for remote detection of C. diff toxins, *Sci. Adv.*, 2019, 5(1), eaau9650.
10 L. Gloag, M. Mehdipour, D. Chen, R. D. Tilley and J. J. Gooding, Advances in the application of magnetic nanoparticles for sensing, *Adv. Mater.*, 2019, 31(48), 1904385.
11 J. Wang, R. Cheng, Y. Wang, L. Sun, L. Chen and X. Dai, *et al.*, Surface-imprinted fluorescence microspheres as ultrasensitive sensor for rapid and effective detection of tetracycline in real biological samples, *Sens. Actuators, B*, 2018, 263, 533–542.
12 J. Wang, J. Dai, Y. Xu, X. Dai, Y. Zhang and W. Shi, *et al.*, Molecularly imprinted fluorescent test strip for direct, rapid, and visual dopamine detection in tiny amount of biofluid, *Small*, 2019, 15(1), 1803913.

13 J. Wang, L. Zou, J. Xu, R. Zhang and H. Zhang, Molecularly imprinted fluoroprobes doped with Ag nanoparticles for highly selective detection of oxytetracycline in real samples, *Anal. Chim. Acta*, 2021, 1161, 338326.

14 H. Eskandari, M. Amirzehni, H. Asadollahzadeh, J. Hassanzadeh and P. A. Eslami, MIP-capped terbium MOF-76 for the selective fluorometric detection of cefixime after its preconcentration with magnetic graphene oxide, *Sens. Actuators, B*, 2018, 275(DEC), 145–154.

15 M. Mehrzad-Samarin, F. Faridbod, A. S. Dezfuli and M. R. Ganjali, A novel metronidazole fluorescent nanosensor based on graphene quantum dots embedded silica molecularly imprinted polymer, *Biosens. Bioelectron.*, 2016, 618.

16 S. Huang, M. Guo, J. Tan, Y. Geng, J. Wu and Y. Tang, *et al.*, Novel fluorescence sensor based on all-inorganic perovskite quantum dots coated with molecularly imprinted polymers for highly selective and sensitive detection of omethoate, *ACS Appl. Mater. Interfaces*, 2018, 10(45), 39056–39063.

17 M. Fizir, P. Dramou, N. S. Dahiru, W. Ruya, T. Huang and H. He, Halloysite nanotubes in analytical sciences and in drug delivery: a review, *Microchim. Acta*, 2018, 185(8), 1–33.

18 M. Wang, M. Gao, L. Deng, X. Kang, L. Yang and T. Quan, *et al.*, Composite material based on carbon dots and molecularly imprinted polymers: a facile probe for fluorescent detection of 4-nitrophenol, *NANO*, 2020, 15, 2050105.

19 H. Liu, L. Ding, L. Chen, Y. Chen, T. Zhou and H. Li, *et al.*, A facile, green synthesis of biomass carbon dots coupled with molecularly imprinted polymers for highly selective detection of oxytetracycline, *J. Ind. Eng. Chem.*, 2019, 69, 455–463.

20 L. Sha, M. Zhu, F. Lin, X. Yu, L. Dong and L. Wu, *et al.*, Stable DNA Aptamer–Metal–Organic Framework as Horseradish Peroxidase Mimic for Ultra-Sensitive Detection of Carcinoembryonic Antigen in Serum, *Gels*, 2021, 7(4), 181.

21 M. Panagiotopoulou, Y. Salinas, S. Beyazit, S. Kunath, L. Duma and E. Prost, *et al.*, Molecularly imprinted polymer coated quantum dots for multiplexed cell targeting and imaging, *Angew. Chem., Int. Ed.*, 2016, 55(29), 8244–8248.

22 B. Li, Z. Zhang, J. Qi, N. Zhou, S. Qin, J. Choo and L. Chen, Quantum dot-based molecularly imprinted polymers on three-dimensional origami paper microfluidic chip for fluorescence detection of phycocyanin, *ACS Sens.*, 2017, 2(2), 243–250.

23 M. Fizir, L. Wei and N. Muchuan, *et al.*, Qbd approach by computer aided design and response surface methodology for molecularly imprinted polymer based on magnetic halloysite nanotubes for extraction of norfloxacin from real samples, *Talanta*, 2018, 184, 266–276.

24 J. Xu, H. Miao, J. Wang and G. Pan, Molecularly Imprinted Synthetic Antibodies: From Chemical Design to Biomedical Applications, *Small*, 2020, 16, 1906644.

25 L. Wu, X. Li, H. Miao, J. Xu and G. Pan, State of the art in development of molecularly imprinted biosensors, *View*, 2021, 20200170.

26 J. Pan, W. Chen, Y. Ma and G. Pan, Molecularly imprinted polymers as receptor mimics for selective cell recognition, *Chem. Soc. Rev.*, 2018, 47(15), 5574–5587.

27 R. Rodr´ıguez-Dorado, A. M. Carro, I. Chianella, K. Karim, A. Concheiro and R. A. Lorenzo, *et al.*, Oxytetracycline recovery from aqueous media using computationally designed molecularly imprinted polymers, *Anal. Bioanal. Chem.*, 2016, 408(24), 6845–6856.

28 M. Hu, P. Huang, L. Suo and F. We, Polydopamine-based molecularly imprinting polymers on magnetic nanoparticles for recognition and enrichment of ochratoxins prior to their determination by hplc, *Microchim. Acta*, 2018, 185(6), 300.

29 R. Liu, Q. Cui, C. Wang, X. Wang, Y. Yang and L. Li, Preparation of sialic acid-imprinted fluorescent conjugated nanoparticles and their application for targeted cancer cell imaging, *ACS Appl. Mater. Interfaces*, 2017, 9(3), 3006–3015.

30 S. Wagner, J. Bell, M. Biyikal, K. Gawlitza and K. Rurack, Integrating fluorescent molecularly imprinted polymer (MIP) sensor particles with a modular microfluidic platform for nanomolar small-molecule detection directly in aqueous samples, *Biosens. Bioelectron.*, 2018, 99, 244–250.

31 Z. Zhou, T. Li, W. Xu, W. Huang, N. Wang and W. Yang, Synthesis and characterization of fluorescence molecularly imprinted polymers as sensor for highly sensitive detection of dibutyl phthalate from tap water samples, *Sens. Actuators, B*, 2017, 240, 1114–1122.

32 J. Qi, B. Li, X. Wang, Z. Zhang, Z. Wang, J. Han and L. Chen, Three-dimensional paper-based microfluidic chip device for multiplexed fluorescence detection of Cu^{2+} and Hg2+ ions based on ion imprinting technology, *Sens. Actuators, B*, 2017, 251, 224–233.

33 N. Leibl, K. Haupt, C. Gonzato and L. Duma, Molecularly imprinted polymers for chemical sensing: A tutorial review, *Chemosensors*, 2021, 9(6), 123.

34 A. D. Hudson, O. Jamieson, R. D. Crapnell, K. Rurack, T. C. C. Soares, F. Mecozzi, A. Laude, J. Gruber, K. Novakovic and M. Peeters, Dual detection of nafcillin using a molecularly imprinted polymer-based platform coupled to thermal and fluorescence read-out, *Mater. Adv.*, 2021, 2, 5105–5115.

35 O. Jamieson, T. C. C. Soares, B. A. de Faria, A. Hudson, F. Mecozzi, S. J. Rowley-Neale, C. E. Banks, J. Gruber, K. Novakovic, M. Peeters and R. D. Crapnell, Screen Printed Electrode Based Detection Systems for the Antibiotic Amoxicillin in Aqueous Samples Utilising Molecularly Imprinted Polymers as Synthetic Receptors, *Chemosensors*, 2020, 8, 5.